Electronic Materials Letters (2020) 16:513–519
https://doi.org/10.1007/s13391-020-00239-8

ORIGINAL ARTICLE - ELECTRONICS, MAGNETICS AND PHOTONICS

Electromigration Behavior of Cu Core Solder Joints Under High Current Density

Haksan Jeong[1] · Choong-Jae Lee[1] · Jae-Ha Kim[1] · Jae-yeol Son[1,2] · Seung-Boo Jung[1]

Received: 20 May 2020 / Accepted: 30 July 2020 / Published online: 12 August 2020
© The Korean Institute of Metals and Materials 2020

Abstract
Cu core solder ball (CCSB) is formed by a Cu core surrounded by solder alloy and is used as an interconnection material for 3D packaging. Herein, the electromigration behavior of CCSBs with an organic solderability preservative surface finish is compared with that of Sn–3.0Ag–0.5Cu (SAC) solder joint. The current density and temperature for electromigration test are 0.9×10^4 A/cm^2 and 100 °C, which are in compliance with JEP154. The current density of the solder joint is analyzed using finite element method analysis and maximum current density of the SAC solder joint is 1.1 times higher than the CCSB solder joint. The CCSB solder joint is less affected by the current crowding effect because electrons move through the Cu core located at the center of the solder. A void form in the Cu electrode of the cathode that coincides with the simulated maximum current area of the solder joint. The electromigration reliability of the CCSB solder joint is superior to that of the SAC solder joint.

Graphic Abstract

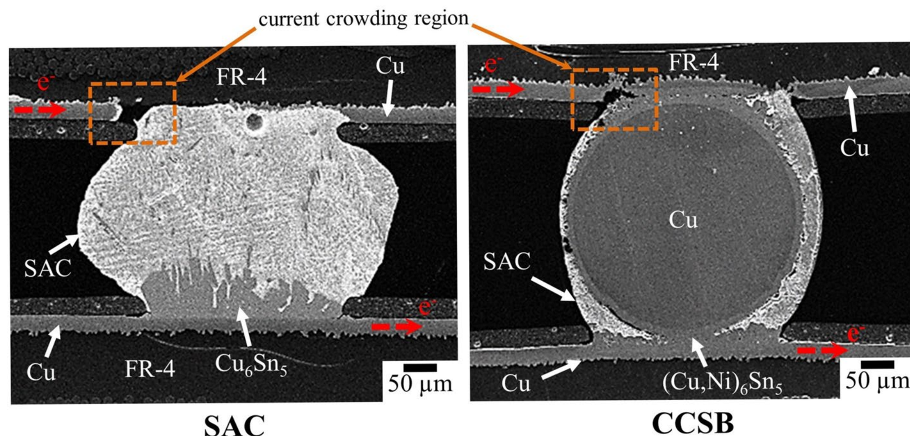

Keywords Cu core solder ball · Sn–3.0Ag–0.5Cu solder · Electromigration · Current crowding effect · Finite element method

✉ Seung-Boo Jung
sbjung@skku.edu

[1] School of Advanced Materials Science and Engineering, Sungkyunkwan University, 2066 Seobu-ro, Jangan-Gu, Suwon 16419, South Korea

[2] MK Electronics, 405, Kumeu-ro, Pogok-eup, Cheoin-gu, Yongin-si, Gyeonggi-do 17030, South Korea

1 Introduction

Electronic package technology required smaller, thinner and higher performance. Among the various electronic package technologies, the ball grid array (BGA) package technology using solder balls for interconnection materials has also been developed according to these trends. The various BGA

packaging structures, such as the chip-scale package, fan-in wafer-level package, package-on-package, Si-interposer 2D package, fan-out wafer-level package, and fan-out panel-level package, have been designed [1–5]. The demand for smaller and higher functional BGA packaging has resulted in an increase in the input and output densities, which can be achieved by increasing the number of electrodes and reducing solder ball sizes [6, 7].

The solder joint used in BGA packaging provides an electrical pathway and mechanical support between Si device and its substrate. The solder material and solder joint shape affect the lifetime of electronic packaging [8–10]. Specifically, decreasing the solder ball size results in electromigration (EM)-induced electrical failures because the current density and temperature of the BGA solder increase with decreasing the size of the solder ball [11]. EM is the phenomenon of an enhanced mass transfer of metal atoms in the direction of the electron flow due to electron momentum transfer resulting from the applied electric current. EM failure of solder joints depends on current crowding, Joule heating, Kirkendall voids, thermomigration, and intermetallic compound (IMC) decomposition of the structure, material, and geometry solder joint in microelectronic packaging [12–15].

The Cu core solder ball (CCSB) comprises a Cu core surrounded by a plated solder layer. CCSB solder joint offers a potential solution for EM failure of solder joints because Cu has an increased electrical and thermal conductivity than conventional solder, thereby possessing better EM failure resistance than Sn. Furthermore, the CCSB solder joint maintains its stand-off height because Cu does not melt when the solder is liquified [16–21].

Herein, the EM behaviors of the Sn–3.0Ag–0.5Cu (SAC) solder joint and CCSB solder joint are investigated. The failure phenomena of these solder joints due to applied current stress is analyzed using the 3D-finite element method (FEM) analysis and microstructures are observed using field emission scanning electron microscopy (FE-SEM).

2 Experimental Procedures

The diameter of both CCSB and SAC solder balls was 280 μm, whereas that of the Cu core in the CCSB was 220 μm. Ni and SAC layers were coated around the Cu core via electroplating. The Ni layer provided a diffusion barrier to eliminate the Kirkendall void between the Cu core and SAC layer. The thickness of the Ni layer and SAC layers was 2 and 28 μm, respectively.

The test kit was a solder mask defined-type flame retardant-4 (FR-4) board and component. The opening size of the bonding pad was 200 μm with an organic solderability preservative (OSP) surface finish. The daisy chain of the test kit was designed in compliance with JEP154, as shown in Fig. 1a. The solder ball was selected and placed on the opening pad. To form a solder ball for the BGA component, the reflow process was performed at the peak temperature of 260 °C for 5 min using a four-zone IR reflow machine (RF-430-N2, Japan Pulse Laboratory Co. Ltd., Japan).

The solder joints were applied at the current density of 0.9×10^4 A/cm^2 at 100 °C, which was calculated based on half of the under-bump metallization (UBM) opening area. Then, FEM analysis was conducted to investigate the current density distribution on the solder joints that are subjected to current stressing condition. As shown in Fig. 1b, the model contained only the daisy-chained solder joint and Cu patterns on the FR-4 substrate. The FR-4 substrate and component in the experimental structure were neglected to simplify the analysis. We assumed that electrons flow from the top to bottom electrode; therefore, the electric current flows in the opposite direction. The number of nodes was 1,792,923 to 1,965,194 depending, and the number of elements was from 880,152 to 1,078,085. The number of nodes and elements was depending on the existence of the Cu core. The electrical resistivity of Cu and SAC assumed isotropic behavior. Table 1 lists the electrical properties of the solder joint [22]. The microstructure of the solder joint under the current stress was observed using SEM and energy dispersive X-ray spectroscope (EDX).

Table 1 Electrical properties of the solder joints.

Material	Isotropic resitivity (Ohm m)
SAC	1.29E−07
Cu	1.69E−08

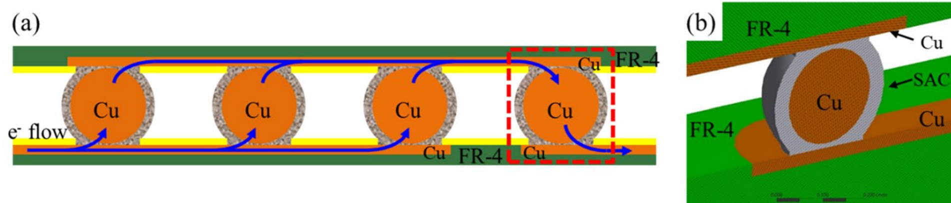

Fig. 1 **a** Schematic of the daisy chain for the electromigration test and **b** cross-sectional plane of the model of electromigration of the CCSB joint

3 Results and Discussion

The 3D-FEM analysis was conducted to determine the failure location due to EM in the solder joints. Figure 2 shows the simulated current density of the solder joint at an applied current density of 0.9×10^4 A/cm^2. The current density was observed to be the highest at the solder joint near the Cu electrode, as seen in Fig. 2, where the electrons experience significant current crowding [22, 23]. Figure 2a, d show that the electrical current flows through the Cu core instead of the solder matrix because the electrical conductivity of Cu is higher than that of the SAC solder joint. As shown in Fig. 2b, e, the simulated maximum current density of the SAC and CCSB solder joints are 2.93×10^6 and 2.66×10^6 A/cm^2, respectively. Maximum current density of the CCSB solder joint is about 10% lower than that of the SAC solder joint. Figure 2c, f indicate that the current density of the solder joint is concentrated at the edge of the opening. However, in the case of the CCSB solder joint, the second-highest current density of 1.36×10^5 A/cm^2 is located at the center of the UBM opening. The electrical resistivity of Cu was much lower than that of SAC. The electron mainly moves to lowest electrical resistance path. Therefore, the electron was moves along the Cu core, even though the distance of electrons movement is longer. In this reason, the current distribution of CCSB joint was spread from the edge of solder joint to Cu electrode and Cu core, as shown in Fig. 2d, f.

The EM Cu flux in Sn ($J_{\mathrm{Cu,\,EM}}$) is related to the current density, [24] and $J_{\mathrm{Cu,EM}}$ is expressed as follows:

$$J_{\mathrm{Cu,EM}} = C_{Cu}\frac{D_{Cu}}{kT}Z^{*}e\rho_{Sn}j,$$

where C_{Cu}, D_{Cu}, and Z^{*} was the concentration, diffusion coefficient, and effective charge number of Cu in Sn, respectively. T is the absolute temperature, k is the Boltzmann constant, e is the electron charge, and j is the current density. When the temperature was same, $J_{\mathrm{Cu,\,EM}}$ was proportional to the j. From the result of FEM analysis, the $J_{\mathrm{Cu,\,EM}}$ of SAC solder joint was 10% higher than that of CCSB solder joint. EM reliability of CCSB solder joint is expected to improve due to the elimination of the current crowding effect by the Cu core.

Figure 3 shows the microstructure of the solder joints after the reflow process. The Cu core of the CCSB solder joint was located in the center. The IMC of the SAC solder joint at the interface between the solder matrix and Cu electrode was a scalloped-type Cu_6Sn_5 IMC comprising 55.0 at.% of Cu and 45.0 at.% of Sn according to the EDX analysis. The $(Cu,Ni)_6Sn_5$ IMC formed at the CCSB solder joint; from EDX spot analysis, its composition on the Cu electrode was determined as 54.3 at.% of Cu, 2.7 at.% of Ni, and 43.0 at.% of Sn. Furthermore, the $(Cu,Ni)_6Sn_5$ IMC on the Cu core comprised 45.3 at.% of Cu, 8.2 at.% of Ni, and 46.5 at.% of Sn. A previous study demonstrated that when the Cu concentration of the solder was 0.5 wt.%, the Cu_6Sn_5-based IMC was formed from the reaction between the SAC and Ni electrodes [25]. In the case of $(Cu,Ni)_6Sn_5$ IMC on the Cu core, the Cu contents were higher than that

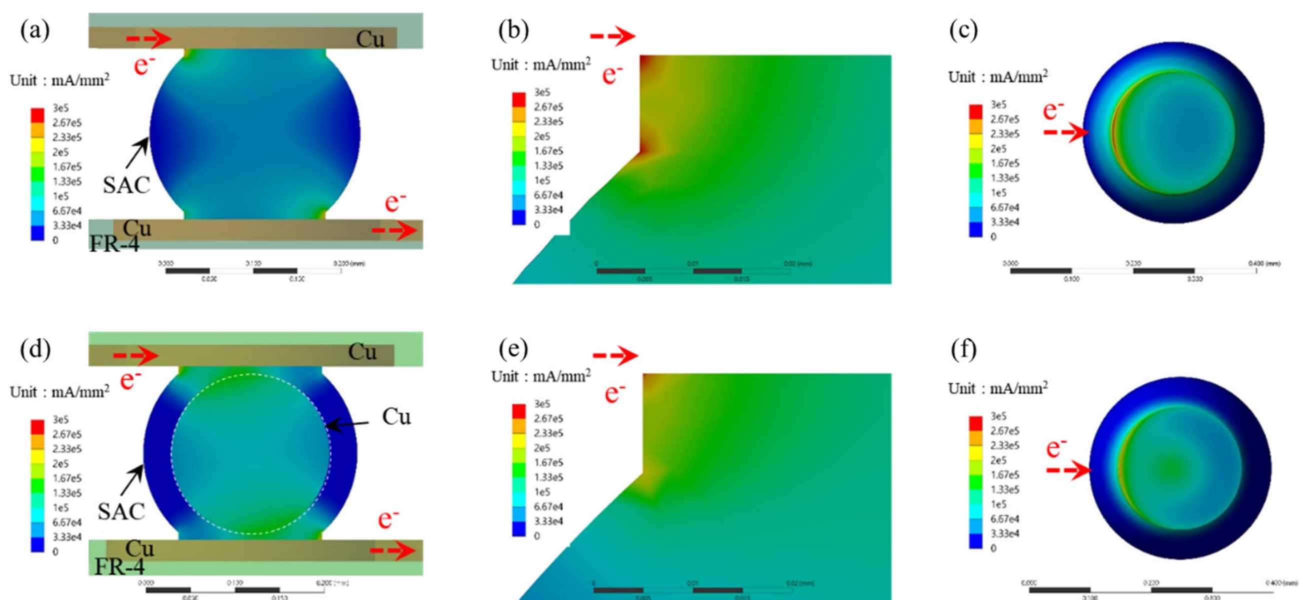

Fig. 2 Contour plots of the current density for **a–c** SAC and **d–f** CCSB solder joints with a current density of 0.9×10^4 A/cm^2. **a**, **d** Whole solder joint, **d**, **e** current crowding region, and **c**, **f** top view of the solder joint

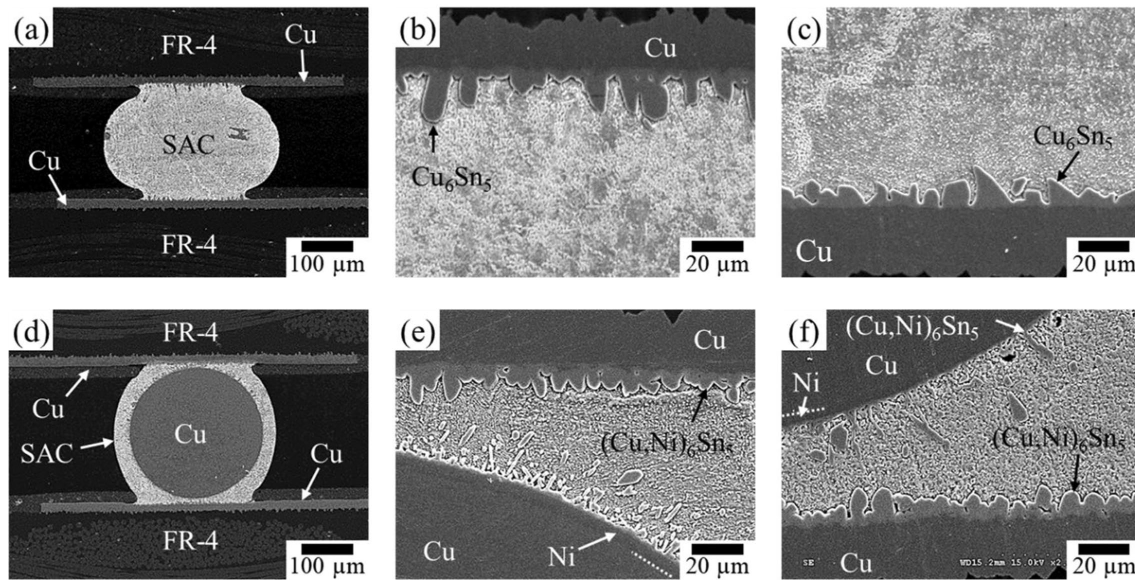

Fig. 3 Cross-sectional SEM micrographs of the **a**–**c** SAC joint and **d**–**f** CCSB joint after the reflow process. **a**, **d** Solder joint, (b, e) cathode, and (c, f) anode

of the Ni contents because the formation of the Cu–Sn IMC prevented the reaction between Ni and Sn [26, 27].

Figure 4 shows the microstructure of the SAC solder joints under the applied current density of 0.9×10^4 A/cm^2 at 100 °C. During the EM test, the thickness of the Cu_6Sn_5 IMC at the anode was relatively thick than that of the Cu_6Sn_5 IMC at the cathode, which was dissolved into the solder matrix by electron current stressing [28]. The Cu_6Sn_5 IMC on the anode grew because migrated Cu from the cathode reacted with Sn at the anode [23]. Also, as shown in Fig. 4c, d, at the cathode, the Cu electrode was consumed during the EM test and a void was observed. The Cu electrode in the cathode provided an entrance through which the electrons could flow in, thereby dissolving the Cu into the solder [12]. The void formed at the entrance where the current crowding occurred most significantly, as seen in Figs. 2b and 4c.

Figure 5 shows the microstructure of the CCSB solder joints under the applied current density of 0.9×10^4 A/cm^2 at 100 °C. The IMC at the anode and Cu core increased with an increase in the current stress time. The Sn in the solder matrix reacted with the migrated Cu; therefore, the IMC on the Cu core also increased. The CCSB solder joint failed due to the formation of a void at the cathode because the Cu was consumed by EM. However, this void is not observed although the CCSB solder joints underwent the EM test for 10 h. Park et al. [15] reported that the Cu was consumed at the cathode due to the polarity effect, wherein the Cu was driven by the electron flow direction during the EM test. Therefore, Cu migrated to the anode following the electron direction. From Fig. 2b, e show that the simulated maximum current density of the CCSB solder joint is lower than that of the SAC solder joint. Therefore, the Cu consumption in the SAC solder joint was more than that in the CCSB solder joint, as shown in Figs. 4c and 5c.

During the EM test, the electrical resistance of both solder joints increased until failure, as shown in Fig. 6a. The resistance change in the CCSB solder joint was less than that in the SAC solder joint. Although a void was formed, it did not fail because the electron flowed through the contact area between the Cu electrode on the cathode and solder. However, the resistance increased because the void reduced the contact area; therefore, the solder joint was affected more by the current crowding effect [23, 29]. As seen in Fig. 6b, the times to failure (TTF) of the CCSB and SAC solder joints were 31.2 and 18.0 h, respectively. Due to the reduced current crowding effect in the CCSB by the Cu core, the TTF of CCSB was 1.73 times longer than that of the SAC solder joint. Therefore, the EM lifetime of the CCSB solder joint was observed to be longer than that of the SAC solder joint without a Cu core.

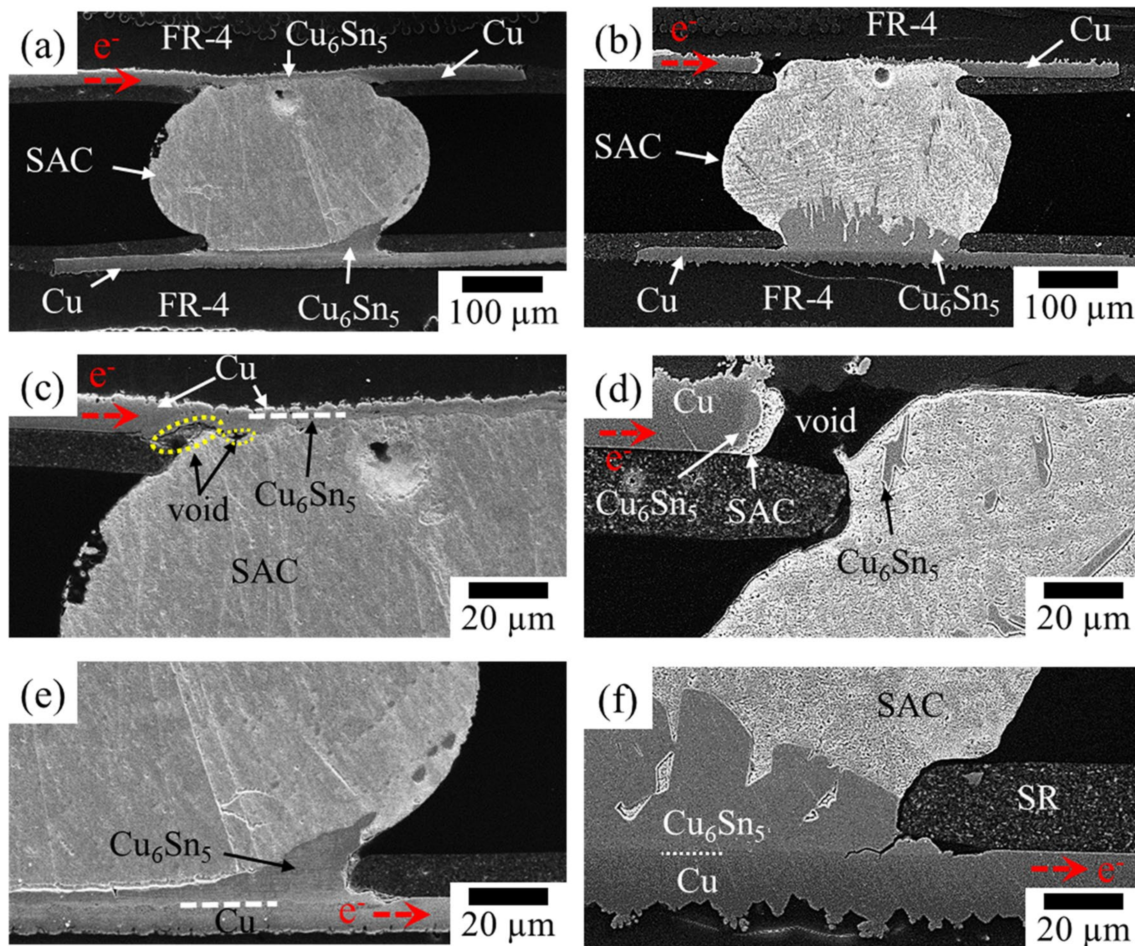

Fig. 4 Cross-sectional SEM micrographs of the SAC joint at a current density of 0.9×10^4 A/cm^2 **a**, **c**, **e** after 10 h at 100 °C and **b**, **d**, **f** after the time to failure. **a**, **b** SAC joint, **c**, **d** magnified cathode, and **e**, **f** anode

4 Conclusion

The EM behaviors of a CCSB solder joint were investigated at a high current density of 0.9×10^4 A/cm^2 at 100 °C. The current densities of the SAC and CCSB solder joints were simulated using FEM, and the highest current density region for both solder joints occurred at the edge of the solder joint near the Cu electrode. The maximum simulated current density of the CCSB solder joint was lower than that of the SAC solder joint because electrical current flowed through the Cu core. At the cathode of both the solder joints, the Cu electrode was consumed and a void formed during the EM test. However, the void at the CCSB solder joint was formed later than that in the SAC solder joint because of a reduced electron crowding effect, thereby resulting in a 1.73 times-longer TTF of the CCSB solder joint than that of the SAC solder joint.

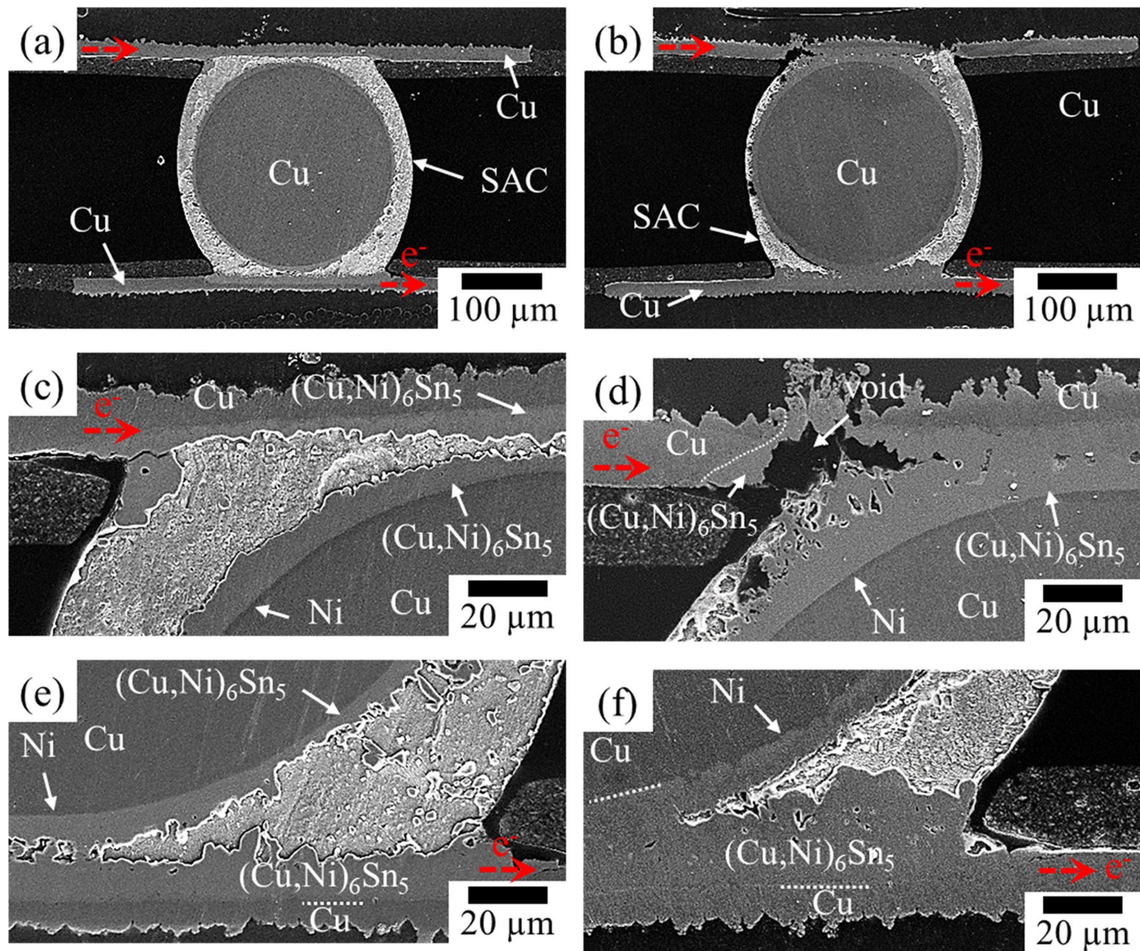

Fig. 5 Cross-sectional SEM micrographs of the CCSB joint with a current density of 0.9×10^4 A/cm^2 **a**, **c**, **e** after 10 h at 100 °C and **b**, **d**, **f** after the time to failure. **a**, **b** CCSB joint, **c**, **d** magnified cathode, and **e**, **f** anode

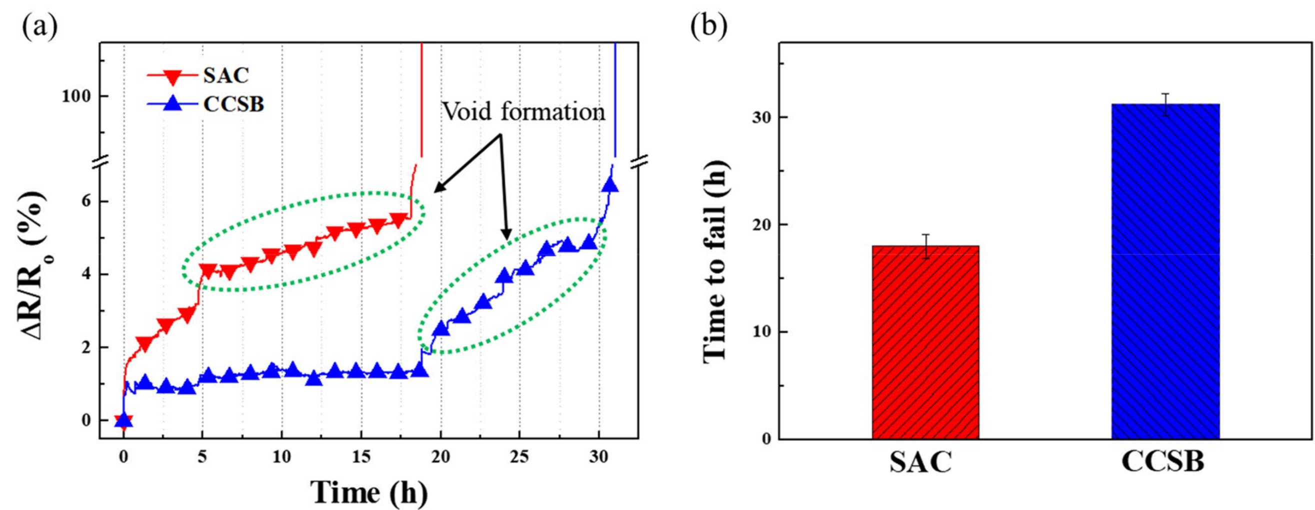

Fig. 6 Result of electromigration of the SAC joint and CCSB joint. **a** $\Delta R/R_0$ versus time of the solder joints at 0.9×10^4 A/cm^2 at 100 °C, **b** times to failure after the electromigration test

Acknowledgements This research was supported by the Basic Science Research Program through the National Research Foundation of Korea (NRF) funded by the Ministry of Education (No. 2019R1A6A1A03033215). This material is based upon work supported by the Ministry of Trade, Industry & Energy (MOTIE, Korea) under Industrial Technology Innovation Program. No.20006956, 'Development of underfill material and package module with high thermal-shock (≥ 2000 cycles) and mechanical drop reliability for mobile applications'.

Compliance with Ethical Standards

Conflict of interest The authors declare that they have no known competing financial interests or personal relationships that could have appeared to influence the work reported in this paper.

References

1. Lau, J.H.: Recent advances and trends in fan-out wafer/panel-level packaging. J. Electron. Packag. **141**(4), 040801 (2019)
2. Lau, J.H.: Recent advances and trends in heterogeneous integrations. J. Microelectron. Electron. Packag. **16**, 45–77 (2019)
3. Che, F.X., Yamamoto, K., Rao, V.S., Sekhar, V.N.: Panel warpage of fan-out panel level packaging using RDL-first technology. IEEE Trans. Compon. Packag. Manuf. Technol. **10**, 304–313 (2019)
4. Tsai, C.H., Liu, S.W., Chiang, K.N.: Warpage analysis of fan-out panel-level packaging using equivalent CTE. IEEE Trans. Device Mater. Reliab. **20**, 51–57 (2019)
5. Lau, J.H., Li, M., Qingqian, M.L., Chen, T., Xu, I., Yong, Q.X., Cheng, Z., Fan, N., Kuah, E., Li, Z., Tan, K.H., Cheung, Y.M., Ng, E., Lo, P., Kai, W., Hao, J., Wee, K.S., Ran, J., Xi, C., Beica, R., Lim, S.P., Lee, N.C., Ko, C.T., Yang, H., Chen, Y.H., Tao, M., Lo, J., Lee, R.S.W.: Fan-out wafer-level packaging for heterogeneous integration. IEEE Trans. Compon. Packag. Manuf. Technol. **8**, 1544–1560 (2018)
6. Mittal, J., Lin, K.L.: Carbon nanotube-based interconnections. J. Mater. Sci. **52**, 643–662 (2017)
7. Datta, M.: Manufacturing processes for fabrication of flip-chip micro-bumps used in microelectronic packaging: an overview. J. Micromanuf. **3**(1), 69–83 (2020)
8. Ha, S.S., Ha, S.O., Yoon, J.W., Kim, J.W., Ko, M.K., Kim, D.G., Kim, S.J., Hong, T.H., Jung, S.B.: Solder joint reliability in flip chip package with surface treatment of ENIG under thermal shock test. Met. Mater. Int. **15**, 655–660 (2009)
9. Noh, B.I., Yoon, J.W., Jung, S.B.: Effects of underfill materials and thermal cycling on mechanical reliability of chip scale package. IEEE Trans. Compon. Packag. Technol. **32**, 633–638 (2009)
10. Yoon, J.W., Back, J.H., Jung, S.B.: Sequential interfacial reactions of SAC305 solder joints with thin ENEPIG surface finishes. Surf. Interface Anal. **50**, 1046–1050 (2018)
11. Kim, J.H., Lee, Y.C., Lee, S.M., Jung, S.B.: Effect of surface finishes on electromigration reliability in eutectic Sn–58Bi solder joints. Microelectron. Eng. **120**, 77–84 (2014)
12. Kim, J.M., Jeong, M.H., Yoo, S., Park, Y.B.: Effects of surface finishes and current stressing on interfacial reaction characteristics of Sn–3.0Ag–0.5Cu solder bumps. J. Electron. Mater **41**, 791–799 (2012)
13. Kim, S.H., Park, G.T., Park, J.J., Park, Y.B.: Effects of annealing, thermomigration, and electromigration on the intermetallic compounds growth kinetics of Cu/Sn–2.5 Ag microbump. J. Nanosci. Nanotechnol. **15**, 8593–8600 (2015)
14. Jang, J.W., Ramanathan, L.N., Tang, J., Frear, D.R.: Secondary current crowding effect during electromigration of flip-chip solder joints. J. Electron. Mater. **37**, 185–188 (2008)
15. Kim, S.H., Kim, J.M., Yoo, S., Park, Y.B.: Effects of surface finishes and current stressing on the interfacial reaction characteristics of Sn–1.2 Ag–0.7 Cu–0.4 In solder bumps. Curr. Appl. Phys. **13**, S103–S107 (2013)
16. Kim, Y., Choi, H., Lee, H., Shin, D., Moon, J., Choe, H.: Fracture behavior of Cu-cored solder joints. J. Mater. Sci. **46**, 6897–6903 (2011)
17. Chen, C.M., Lin, H.C.: Interfacial reactions and mechanical properties of ball-grid-array solder joints using Cu-cored solder balls. J. Electron. Mater. **35**, 1937–1947 (2006)
18. Mu, W., Zhou, W., Li, B., Wu, P.: Janus-faced Cu-core periphery formation and Bi phase redistribution under current stressing in Cu-cored Sn58Bi solder joints. J. Alloys Compd. **584**, 483–486 (2014)
19. Kim, Y., Choi, H., Lee, H., Shin, D., Cho, J., Choe, H.: Improved reliability of copper-cored solder joints under a harsh thermal cycling condition. Microelectron. Reliab. **52**, 1441–1444 (2012)
20. Uenishi, K., Kohara, Y., Sakatani, S., Saeki, T., Kobayashi, K.F., Yamamoto, M.: Melting and joining behavior of Sn/Ag and Sn–Ag/Sn–Bi plating on Cu core ball. Mater. Trans. **43**, 1833–1839 (2002)
21. Sa, X., Wu, P.: Microstructure evolution of Cu-cored Sn solder joints under high temperature and high current density. J. Electron. Mater. **42**, 2641–2647 (2013)
22. Ha, S.S., Kim, J.W., Yoon, J.W., Ha, S.O., Jung, S.B.: Electromigration behavior in Sn–37Pb and Sn–3.0Ag–0.5Cu flip-chip solder joints under high current density. J. Electron. Mater. **38**, 70–77 (2009)
23. Kim, D.G., Moon, W.C., Jung, S.B.: Effects of electromigration on microstructural evolution of eutectic SnPb flip chip solder bumps. Microelectron. Eng **83**, 2391–2395 (2006)
24. Ho, P.S., Kwok, T.: Electromigration in metals. Rep. Prog. Phys. **52**, 301 (1989)
25. Ho, C.E., Tsai, R.Y., Lin, Y.L., Kao, C.R.: Effect of Cu concentration on the reactions between Sn–Ag–Cu solders and Ni. J. Electron. Mater. **31**, 584–590 (2002)
26. Yoon, J.W., Jung, S.B.: Effect of surface finish on interfacial reactions of Cu/Sn–Ag–Cu/Cu (ENIG) sandwich solder joints. J. Alloys. Compd. **448**, 177–184 (2008)
27. Yoon, J.W., Moon, W.C., Jung, S.B.: Interfacial reaction of ENIG/Sn–Ag–Cu/ENIG sandwich solder joint during isothermal aging. Microelectron. Eng. **83**, 2329–2334 (2006)
28. Park, G.-T., Lee, B.-R., Son, K., Park, Y.-B.: Ni barrier symmetry effect on electromigration failure mechanism of Cu/Sn–Ag microbump. Electron. Mater. Lett. **15**, 149–158 (2019)
29. Wang, F., Chen, H., Li, D., Zhang, Z., Wang, X.: Interfacial behaviors in Cu/molten Sn–58Bi/Cu solder joints under coupling with thermal and current stressing. Electron. Mater. Lett. **15**, 36–48 (2019)

Publisher's Note Springer Nature remains neutral with regard to jurisdictional claims in published maps and institutional affiliations.